Journal of Structural Geology 31 (2009) 791–801

Contents lists available at ScienceDirect

Journal of Structural Geology

journal homepage: www.elsevier.com/locate/jsg

On spherical nanoindentations, kinking nonlinear elasticity of mica single crystals and their geological implications

S. Basu, A. Zhou, M.W. Barsoum*

Department of Materials Science and Engineering, Drexel University, Philadelphia, PA 19104, USA

ARTICLE INFO

Article history:
Received 18 March 2008
Received in revised
form 4 May 2009
Accepted 4 May 2009
Available online 20 May 2009

Keywords:
Deformation in mica
Spherical nanoindentation
Indentation stress–strain
Kink bands
Nonlinear elasticity

ABSTRACT

In this paper, we show, using cyclic spherical nanoindentation experiments, that the deformation mechanisms in mica, including basal plane ruptures and delaminations, can be explained by invoking the presence of mobile dislocation walls, and incipient and regular kink bands. Our results clearly show that the energy dissipated or that was stored during the deformation of muscovite depends critically on its previous deformation history and/or the pre-existing defect concentration. Once nucleated, the dislocation-based incipient kink bands are believed to be responsible for the nonlinear elastic deformation and hysteretic loops obtained during cyclic loading. Moreover, a model is presented to estimate the number and distribution of dislocations and the energy consumed in their motion under the indenter. From the model, we also estimate the critical resolved shear stress for the motion of basal plane dislocations under the indenter. The implications of this work can be extended beyond mica to understand the nonlinear hysteretic deformation in other geological formations dominated by layered minerals.

1. Introduction

The importance of micas, and other layered silicates, in the deformation of geologic formations has long been appreciated (Bell and Wilson, 1981; Christoffersen and Kronenberg, 1993; Kronenberg et al., 1990; Mares and Kronenberg, 1993; Shea and Kronenberg, 1993). These layered minerals are geologically abundant and typically deform by dislocation glide along their basal planes under modest shear stresses, which renders them relatively weak and deformable (Kronenberg et al., 1990; Mares and Kronenberg, 1993; Shea and Kronenberg, 1993). It has also long been appreciated that kinking is a favored mode of deformation mechanism in rocks and especially micaceous solids (Bell and Wilson, 1981; Christoffersen and Kronenberg, 1993; Kronenberg et al., 1990; Meike, 1989). Kink bands, KBs, have been observed in micas, at many scales, from the macroscopic, to the transmission electron microscope, TEM, level (Bell and Wilson, 1981; Meike, 1989).

Mica belongs to a family of layered compounds that are formed by sheets of negatively charged silicate layers bonded together by interlayer cations, such as sodium or potassium. The interlayer bonding is typically weak compared to the in-plane bonds of the silicate sheets. At 61 GPa, the elastic constant in the direction perpendicular to the layers (c_{33}) is roughly 4 times the elastic shear constant between the layers (c_{44}) at 15 GPa (McNeil and Grimsditch, 1993).

On another front, the mechanical response of many rocks is known to exhibit hysteretic nonlinear elastic behavior and discrete memory (Guyer and Johnson, 1999; Guyer et al., 1995; Holcomb, 1981; McCall and Guyer, 1994). Recently, we have shown that the vast majority of plastically anisotropic solids can deform in a fully reversible, but nonlinear fashion (Barsoum et al., 2004a, 2004b; Barsoum et al., 2003; Zhou et al., 2008, 2006), in the process of forming dislocation-based kink bands. Typically the sole requirement for a solid to be kinking nonlinear elastic, KNE, is plastic anisotropy – a simple measure of which is a high aspect ratio of the unit cell structure. For example, we have shown that when the ratio between long and short axes of a hexagonal unit cell (c/a ratio) is greater than ≈ 1.4, solids tend to be KNE.

KNE solids are characterized by the formation of fully reversible, reproducible, hysteretic stress–strain loops. The latter are caused by incipient kink bands, IKBs, that are nothing but parallel dislocation loops, confined to two dimensions, stacked one on top of another in form of an ellipsoid, with long and short dimensions of 2α and 2β, respectively (Fig. 1a) (Barsoum et al., 2003). The IKB geometry is such that the loops remain extended *only* if a load is applied. Removal of the load results in their spontaneous annihilation (Frank and Stroh, 1952). It is the to-and-fro motion of these dislocations that we believe is responsible for the hysteretic

* Corresponding author. Tel.: +1 267 307 5114; fax: +1 215 895 6760.
E-mail address: barsoumw@drexel.edu (M.W. Barsoum).

0191-8141/$ – see front matter © 2009 Elsevier Ltd. All rights reserved.
doi:10.1016/j.jsg.2009.05.008

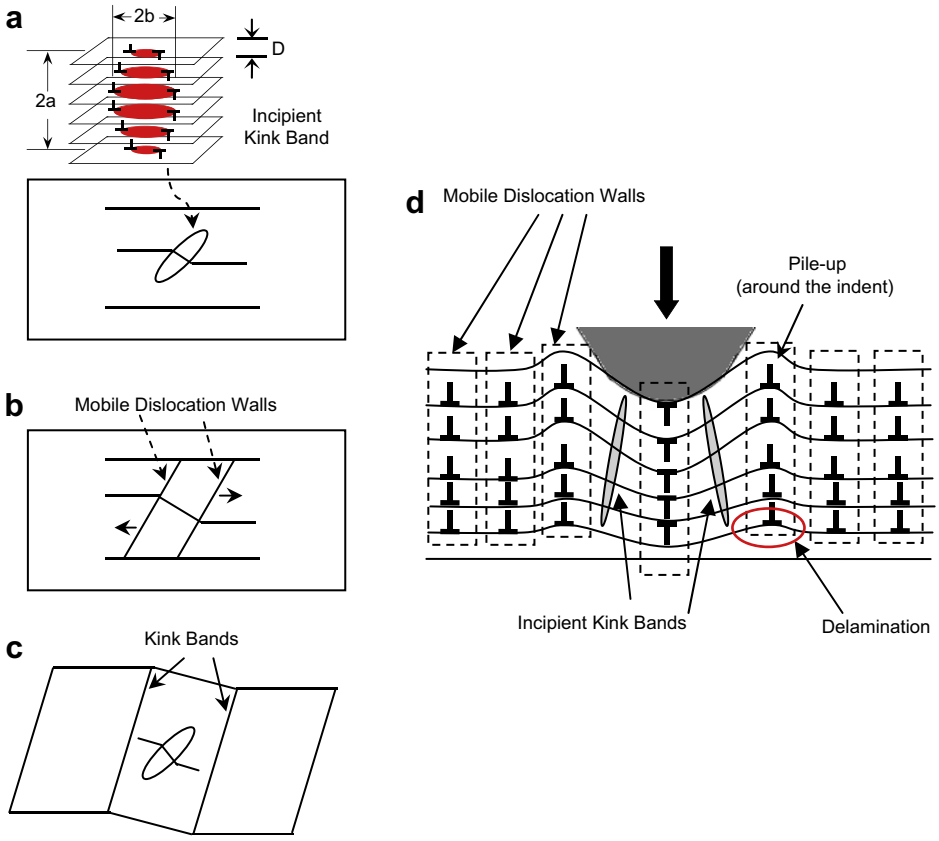

Fig. 1. a) Geometry and schematic of formation of an incipient kink band (IKB) under stress in a layered crystal. b) Formation of mobile dislocation walls (MDWs) by dissociation of IKB at greater stresses. The MDWs move away from each other. c) Formation of permanent kink bands (KBs) at greater stresses than (b). Note the formation of new IKB inside the smaller domain, enclosed by the KBs. d) Cross-sectional schematic of nested MDWs formed under the spherical indenter. Note pile-up around the indent and the IKBs that form inside the domains.

stress–strain loops (see below). Due to their very nature, IKBs cannot exist ex-situ because they can only exist under load.

At greater stresses, and/or temperatures, the IKBs dissociate into mobile dislocation walls (MDW) and a repetition of this process causes the formation of permanent kink bands (KB) (Figs. 1a–c) (Barsoum and El-Raghy, 1999; Barsoum et al., 1999; Farber et al., 1999; Hess and Barrett, 1949). Mobile dislocation walls, MDWs, are low-angle grain boundaries and the dislocations forming these walls glide on parallel crystallographic planes in response to a shear stress.

Since mica is plastically quite anisotropic, it is not surprising that it is a KNE solid. Using mostly cyclic nanoindentation experiments in mica single crystals, we showed that IKBs play a more important role in the deformation of mica than has been appreciated (Barsoum et al., 2004b). When loaded up to 100 mN, the response was characterized by a first stress–strain cycle that was slightly open; all subsequent cycles to the same load were fully reversible and closed. The large amount of energy dissipation per unit volume per cycle ($\approx$80 MJ/m^3 at 3 GPa) was postulated to result from the to and from motion of basal plane dislocations that make up the IKBs (Barsoum et al., 2004b).

The presence of basal plane dislocations in micas has been known for a long time from the 'percussion' figures of Bauer (1874) and, more recently, from detailed studies by Meike (1989) and Kronenberg et al. (1990). Also, clear evidence of KB formation was obtained from post-indentation characterization by scanning electron microscope, SEM (Barsoum et al., 2004b). As noted above, kinks in mica have been long appreciated, but little was known regarding their nucleation.

The purpose of this paper is to present further evidence confirming that mica is indeed a KNE solid and, more importantly, the effect of defect concentrations on this behavior. Initially, we briefly describe the physics of IKB formation, and the conversion of spherical nanoindentation, NI, load-displacement curves to NI stress–strain curves (Basu et al., 2006b). We also apply our recently developed KNE model to our NI stress–strain results (Barsoum et al., 2005b; Zhou et al., 2008). Lastly, we discuss the implications of our results to geology.

2. Theoretical considerations

2.1. Microscale model: kinking nonlinear elastic deformation

Our recently developed model (Barsoum et al., 2005b; Zhou et al., 2008) is based primarily on a theoretical paper by Frank and Stroh (1952), (F&S), who considered the problem of the growth of a thin elliptical kink with dimensions 2α and 2β, such that $2\alpha >> 2\beta$ (Fig. 1a). Initially, the elliptical kink is comprised of dislocation loops with components of opposite sign, such that as long as the ends are attached they are *attracted* to each other (Fig. 1a). However, because initially they increase the energy of the system, the kinks are subcritical or unstable. Using an energy approach, reminiscent of Griffith's, F&S showed that the remote shear stress, τ, needed to render a subcritical kink band unstable – and hence grow – depended on α:

$$\tau > \tau_t \approx \frac{\sigma_t}{2} \approx \sqrt{\frac{4G^2 b\gamma_c}{2\alpha\pi^2}\ln\left(\frac{b}{\gamma_c w}\right)} \quad (1)$$

where b is the Burgers vector (5.19 Å); G is the shear modulus – for single crystals, G is replaced by c_{44} – and σ_t is a threshold stress; w is related to the width of the dislocations and assumed to be equal to b. γ_c is the critical angle of kinking given by (Frank and Stroh, 1952):

$$\gamma_c = \frac{b}{D} \approx \frac{3\sqrt{3}(1-\nu)\tau_{loc}}{2G} \tag{2}$$

where ν is Poisson's ratio, D is the distance between dislocations in the wall (Fig. 1a) and τ_{loc} is the local shear stress. Assuming $\nu = 0.25$ and $\tau_{loc} \approx G/30$, which implicitly assumes $w = b$, yields a γ_c of 0.065 or $\approx 4°$.

F&S modeled a two dimensional single crystal and assumed, correctly, that once the inequality in Eq. (1) was satisfied, the subcritical kink band would rapidly, and auto-catalytically, grow to the edge of the sample and dissociate into two parallel mobile dislocation walls (MDW) (Fig. 1b). The repetition of this process ultimately leads to the formation of KBs (Fig. 1c) that are irreversible (Barsoum and El-Raghy, 1999; Barsoum et al., 1999; Hess and Barrett, 1949).

An IKB is *fully reversible* upon the removal of the load because of the opposite polarity of two edge components in the dislocation loops comprising it and the elliptical shape of the deformed region that they encompass (Fig. 1a) (Barsoum et al., 2003). Each dislocation loop can be assumed to be comprised of two edge and two screw dislocation segments with lengths, $2\beta_x$ and $2\beta_y$, respectively. Given that we do not understand the IKB nucleation process and as they occur only when the applied stress is $> \sigma_t$, we only model the growth process. In other words, we assume that when $\sigma > \sigma_t$, the IKBs grow by increasing from a critical size, $2\beta_{i,c}$ to $2\beta_i$, according to Frank and Stroh (1952), Zhou et al. (2008),

$$2\beta_x = \frac{2\alpha(1-\nu)}{G\gamma_c}\frac{\sigma}{2} \tag{3}$$

for the edge components, and

$$2\beta_y = \frac{2\alpha}{G\gamma_c}\frac{\sigma}{2} \tag{4}$$

for the screw components.

The nonlinear strain, ε_{NL} due to the growth of these elliptical IKBs from β_c to β is thus given by (Barsoum et al., 2005b; Zhou et al., 2008):

$$\varepsilon_{NL} = \frac{\Delta V N_k \gamma_c}{k_1} = \frac{\pi(1-\nu)N_k\alpha^3}{3k_1G^2\gamma_c}(\sigma^2 - \sigma_t^2) \tag{5}$$

where, N_k is the number of IKBs per unit volume and, k_1 is a factor (assumed to be 2) that converts volumetric strain to linear strain (Zhou et al., 2008). ΔV is the change of volume of the IKB at stress $\sigma > \sigma_t$. The factor, $N_k\alpha^3$, varies between 1 and 6 (Basu et al., 2008) and corresponds to the number of IKBs forming within one domain having a volume of the order of α^3.

If Ω is the energy dissipated by a dislocation line sweeping a unit area, then the area within each stress–strain loop or the energy dissipated per cycle per unit volume, W_d, can be expressed as (Barsoum et al., 2005b; Zhou et al., 2008),

$$W_d = \frac{\pi(1-\nu)N_k\alpha^3}{G^2\gamma_c}\frac{\Omega}{b}(\sigma^2 - \sigma_t^2) \tag{6}$$

As demonstrated herein and in previous work (Barsoum et al., 2004a, 2004b, 2003; Basu and Barsoum, 2007; Basu et al., 2006a; Zhou et al., 2008), the formation of fully reversible, reproducible hysteretic stress–strain loops upon cycling is one of the signatures of IKBs. In deriving Eq. (6), W_d is assumed to be solely due to the movement of IKB-related dislocations, so consequently any motion of dislocations in pile-ups is neglected. With that caveat, Ω/b is a material property that is proportional to, if not identical to, the critical resolved shear stress, CRSS, of the basal plane dislocations comprising the IKBs (Zhou et al., 2008).

An incipient kink boundary is initially two low-angle grain or tilt boundaries of opposite polarities. If such a boundary – of length 2α – is subjected to a shear stress, Stroh (1958) showed that cleavage in a metal single crystal would occur when:

$$\sigma_n\sigma_s \geq \frac{\mu\gamma G}{2\alpha\pi} \tag{7}$$

where σ_n is the applied stress, σ_s the resolved shear stress, γ the surface energy of the cleavage planes, and μ is a numerical constant of the order of unity that depends on the elastic anisotropy of the crystal and the stress state. This mechanism is particularly suited to solids in which the cleavage and slip planes coincide such as mica or Ti_3SiC_2 (Zhen et al., 2005). Eq. (7) is important because it provides a mechanism for the delaminations (failure of interlayer bonds in layered solids) observed in this work. Note that, regardless of the details, the IKB to KB transformation *cannot* occur without delaminations or the presence of a free surface.

The delaminations are also in agreement with earlier observations of deformed micas (Christoffersen and Kronenberg, 1993), where it was shown that – when dislocation climb is difficult – dislocations that glide in a wall configuration are unevenly spaced and hence cause stress concentrations along the boundary, which gives rise to cleavage or delamination cracks. Upon delamination, the IKBs transform into MDWs that are swept away from under the indenter and form a pile-up of material around the indented area (Fig. 1d).

2.2. Conversion of spherical NI load-displacement curves to NI stress–strain curves

NI stress–strain curves are more informative than simple load-displacement curves because of two main reasons. First, the stress–strain response normalizes the load-displacement data by the deformation geometry and, second, it can be directly compared to macroscopic experiments in terms of elastic moduli, yield stresses and strain-hardening, etc. Despite the fact that depth-sensing NI techniques have been around for at least two decades, most researchers eschewed converting the load-displacement results to NI stress–strain curves in general, and in brittle solids in particular. In the following we briefly describe, the procedure that we developed to convert spherical NI load-displacement response to NI stress–strain curves.

Applying a load of P using a spherical indenter of radius, R, results in an elastic penetration depth, h_e (Fig. 2a), relative to the original surface given by (Hertz, 1896):

$$h_e = \left(\frac{3P}{4E^*}\right)^{2/3}\left(\frac{1}{R}\right)^{1/3} \tag{8}$$

where E^* is the reduced modulus given by:

$$\frac{1}{E^*} = \frac{1-\nu_s^2}{E_s} + \frac{1-\nu_i^2}{E_i} \tag{9}$$

The subscripts s and i refer to the specimen and the indenter, respectively. The contact depth, h_c, and the contact radius, a, (Fig. 2a) were determined from (Basu et al., 2006b):

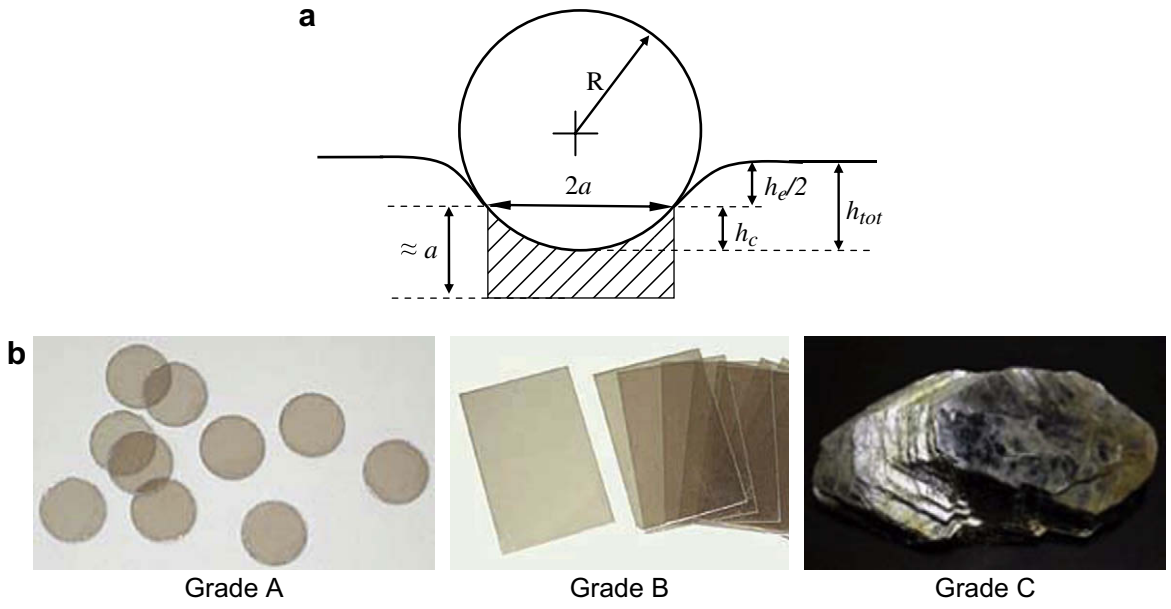

Fig. 2. a) Schematic showing various geometric parameters in spherical indentation that are defined in the main text. b) Photographs of three different grades of mica single crystals.

$$h_c = h_t - \frac{3}{4}\frac{P}{S} \pm \delta \tag{10}$$

$$a = \sqrt{2Rh_c - h_c^2} \tag{11}$$

where h_t is the total displacement and S is the specific stiffness. Initially the parameter δ – which is of the order of few nm's – was used to render the slopes of the stress–strain curves in the elastic regime at low stresses equal to the elastic moduli (Basu et al., 2006b). More recently, we showed that δ is actually related to the effective zero-point of contact (Moseson et al., 2008) and that it mostly affects the slopes of the stress–strain curves in the early elastic regime (Basu et al., 2006b). In other words, δ is an artifact of uneven surfaces. In this work, we used the procedure described by Moseson et al. (2008) to correct for the zero-point, and hence to obtain correct elastic moduli values from the NI stress–strain results.

Once a is determined at each P, the Meyer or indentation stress, $P/\pi a^2$, (Tabor, 1951) is plotted against indentation strain a/R. In the elastic regime (Field and Swain, 1995; Herbert et al., 2000; Hertz, 1896; Johnson, 1985),

$$\frac{P}{\pi a^2} = \frac{4}{3\pi}E^*\left(\frac{a}{R}\right) \tag{12}$$

where the slope of the curve should be proportional to E^* (Basu et al., 2006b; Moseson et al., 2008).

3. Experimental procedure

Cyclic NI experiments were conducted on freshly cleaved mica surfaces that revealed atomically flat basal planes with a nano-indenter (MTS Nanoindenter XP System, MTS Corporation, Oak Ridge, TN) using a 13.5 μm radius sphero-conical diamond tip and the continuous stiffness measurement (CSM) attachment. The tip radius was calibrated with standard amorphous silica and viewed in a scanning electron microscope, SEM (XL30, FEI Corporation, Hillsboro, OR). The tests were conducted under load control at loading rate/load ratio of 0.1 – perpendicular to the basal planes. All tests were performed only after the instrumental drift was below 0.05 nm/s. A few tests were carried out using a 5 μm spherical indenter tip radius.

To study the effect of cycling, typically multiple (mostly 5) indentations were conducted on the same location for a given load. In most cases, the first three cycles resulted in permanent residual displacements, while subsequent cycles were characterized by fully reversible hysteretic loops. In many of the repeat cycles, a small (<10 nm) residual deformation was recorded. By careful calibration with silica, which behaves elastically, we confirmed that these residual values were an artifact of the measurement, most probably due to thermal drift. In other words, the third, and subsequent loops were indeed *fully* reversible. This result was checked by indenting a sample in the same location 30 times. Within the measurement's resolution, no difference was found between the *areas* of the fourth and thirtieth load-displacement loops. To account for this artifact, the *unloading* curves on the fourth and subsequent loadings were forced to coincide with the *unload* curves of the third cycle (Barsoum et al., 2004a, 2004b). The corrected, or shifted load-displacement curves were then converted to stress–strain curves.

Three commercially available natural muscovite single crystals that differed in purity and quality were studied. Based on the amount of initial defects (in terms of porosity and delaminations) and amount of other phases, the grades were classified as A, B and C (Fig. 2). Mica A was the highest purity grade available; B was a slightly lower grade (both obtained from Ted Pella Inc., Redding, CA, commercially available as grades V1 and V2, respectively). The sheets were approx ~150–200 μm thick. The differences between grades A and B are subtle since there was little difference in their transparency (Fig. 2b). Grade C mica (Custer County, SD – Geoprime Earth Materials Co.), on the other hand, had a higher defect population evident from its lack of transparency, attributed to defects such as air pockets, delaminations and inclusions of other phases (Fig. 2b). The grade C sample was a few millimeters thick and was cleaved to expose atomically flat surfaces prior to testing. The post-indent surface features, for all grades, were also observed in a SEM (XL 30, FEI Corporation, Hillsboro, OR).

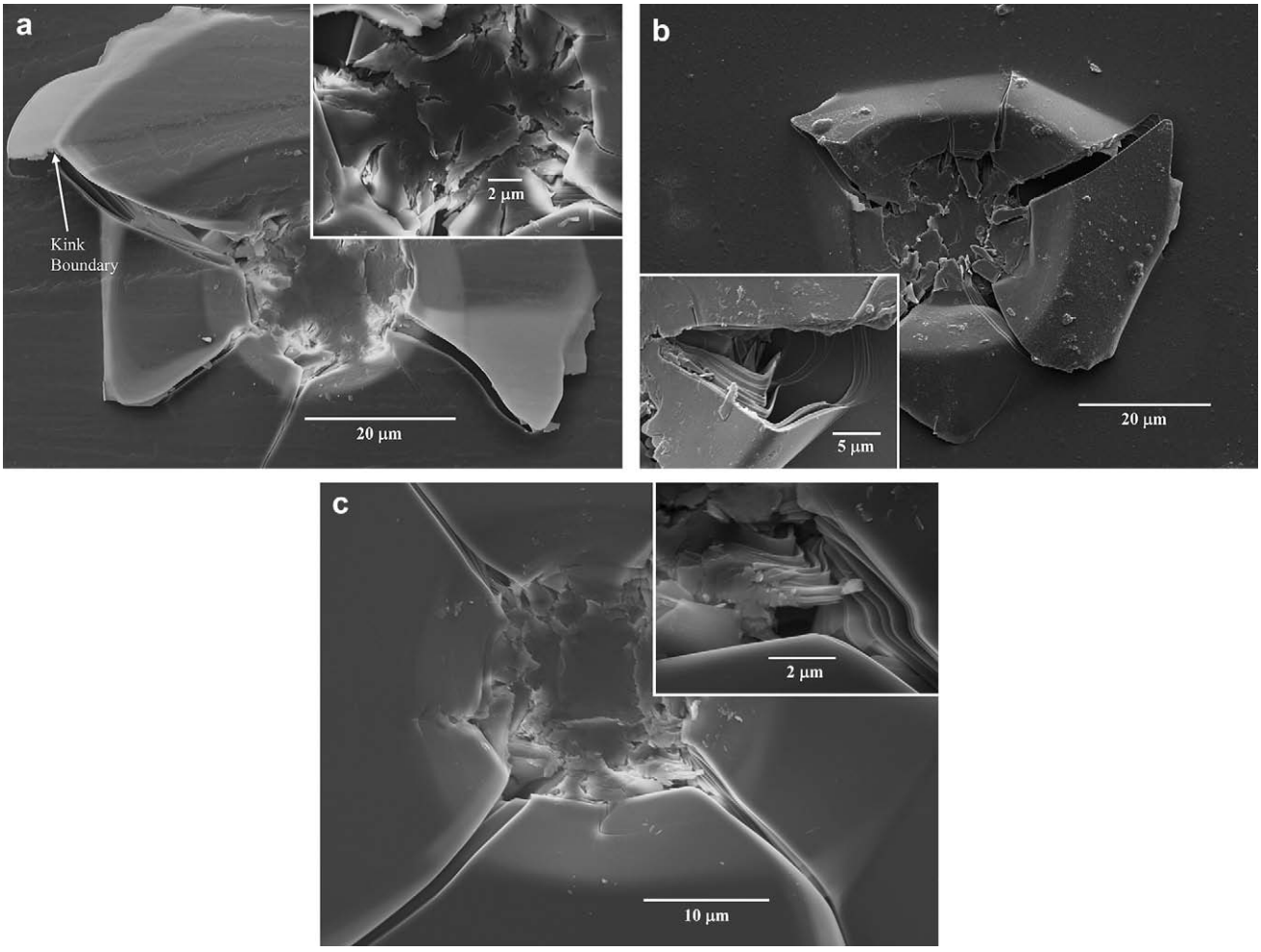

Fig. 3. Scanning electron microscope micrographs of indented regions when the 13.5 μm indenter was loaded up to 500 mN into: a) Grade A mica; Note pile-up and kink boundaries around the indented region. The inset shows a magnified picture of the deformation inside the indented region with extensive delaminations and cracking that occurred during the pop-in event. b) Grade B mica; Note again pile-up and extensive cracking around and inside the indent, respectively. Inset shows a magnified image of a kink boundary that formed around the indented region. c) Grade C mica; inset shows formation of kink boundaries and extensive rotation of basal planes under the indented region.

4. Results

Figs. 3a–c show the surface features and kink band formation surrounding the indents after loading to 500 mN for the different grades of mica. The NI marks are more or less round and sometimes 6 cracks emanate from the indented region (Figs. 3a, b). Examination of Fig. 3 reveals the segmentation of the single crystal into multiple domains, which is a key component in our model and is believed to occur during the pop-in events (see below). This deformation-induced segmentation is similar to that reported by Bell and Wilson (1981) in biotites. Clear evidence for the formation of KBs in the pile-ups around the indented region was seen in all three grades. The massive rotation of some of the lattice planes (inset, Fig. 3c) is unambiguous and striking in its severity.

The deformation behavior depended on the mica grade (Figs. 4a, b). Upon cyclic loading the response of grade A mica was either linear elastic or resulted in fully reversible hysteresis cycles (Fig. 5a), but only *after* sudden and large displacements (Fig. 4b) of the nanoindenter tip, typically referred to hereafter, and in the NI literature, as pop-ins. Pop-ins are manifestations of very rapid deformations associated with the sudden penetration of the NI tip into a surface. Typically, pop-ins in metals are of the order of a few nanometers. The pop-ins observed here would thus be considered extreme.

The elastic behavior and pop-in stresses of grade B were similar to grade A, but resulted in slightly higher W_d values. The deformation of Grade C, on the other hand, produced the largest hysteresis loops and, as important, sometimes exhibited some plastic deformation prior to the pop-ins.

The variability of deformation behavior is clearly evidenced when the pop-in stresses are plotted on a Weibull plot (Fig. 4c), which is a widely used statistical plot to represent variability in failure stresses (Weibull, 1951). Such plots are typically used to estimate probabilities of failure. The Weibull distributions of A and B were quite comparable as both have Weibull moduli of ≈ 8; at 7 ± 1 GPa, and their average pop-in stresses were high. Conversely, the pop-in stresses and Weibull moduli for grade C were significantly lower (see dashed line in Fig. 4c). The results for grade C were from different days and locations on the surface. Interestingly, within a given region in mica C, the Weibull moduli are almost as high as those in grades A and B; the difference between the two regions, however, is significant. Given this variability, each grade is discussed separately.

4.1. Grade A

At least 3 different responses were observed for the deformation of Grade A samples (Figs. 4a and 5)

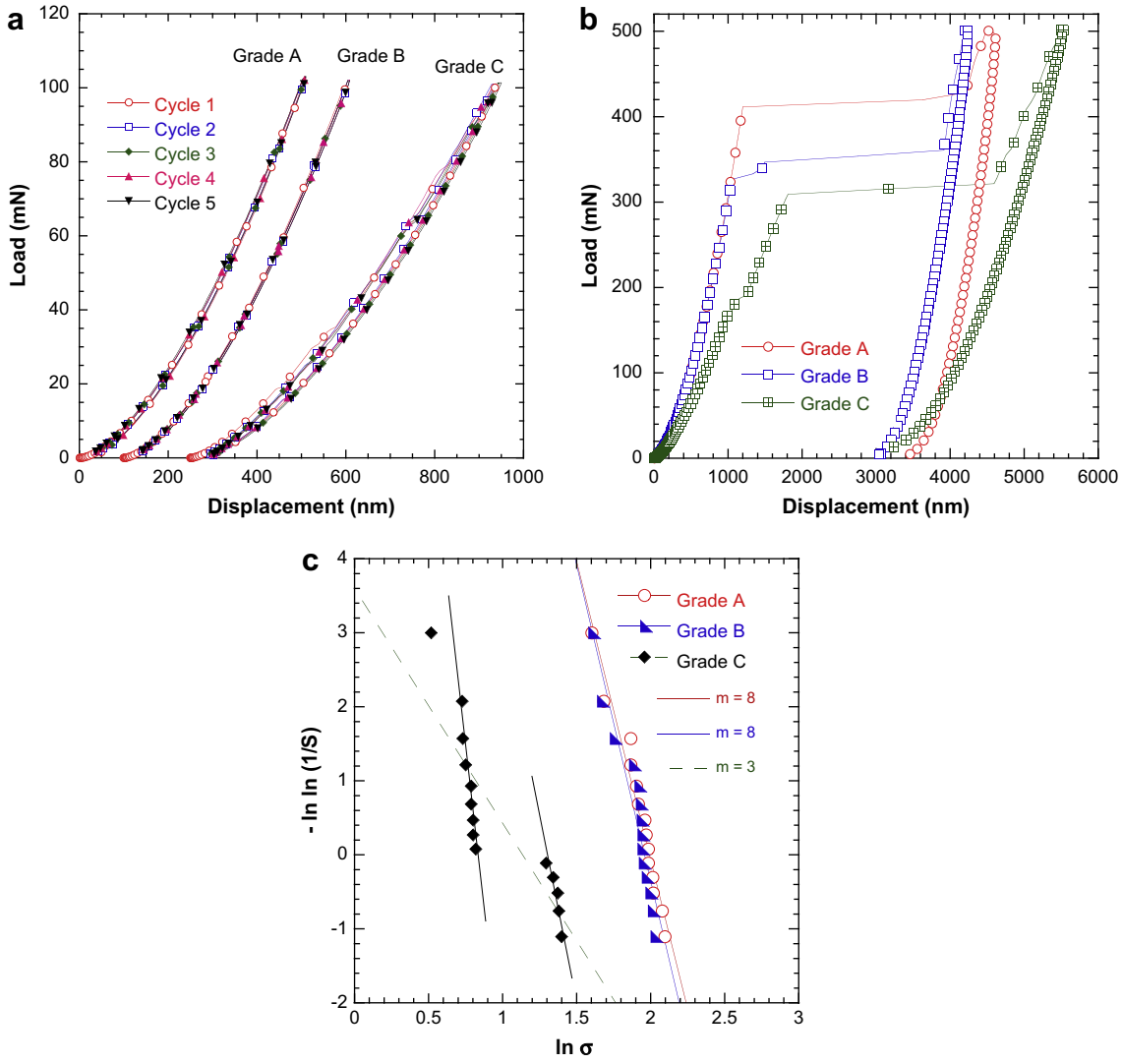

Fig. 4. a) Typical load-displacement curves for the three different grades of mica when the surfaces are indented to a load of 100 mN using a 13.5 μm radius indenter. The curves for grades B and C results are arbitrarily shifted to the right by 100 nm and 250 nm, respectively, for purposes of facilitating comparison. The response of grades A and B is mostly elastic, whereas grade C has small pop-ins during the first cycle and dissipates considerably more energy during repeat cycles. b) Typical load-displacement curves when samples are indented to a load of 500 mN using a 13.5 μm radius indenter. Note the behavior of grades A and B are similar, while grade C exhibits plastic deformation prior to pop-in. c) Weibull plots for pop-in stresses. Grade C exhibited the smallest pop-in stresses and smallest overall Weibull moduli. However, two different regions in the grade C sample had Weibull moduli similar to those for grades A and B.

i. linear elastic up to the largest load possible, viz. 500 mN, (open squares in Figs. 5a, and b). When the load-displacement results were converted to stress–strain curves, the latter confirmed the elastic behavior prior to the pop-ins, as evidenced by slopes that corresponded to an elastic modulus of 61 GPa (dashed inclined line in Fig. 5b). This value, concidentaly or not, of the is identical to the value of c_{33} reported for muscovite mica (McNeil and Grimsditch, 1993).
ii. linear elastic, initially with a modulus of 61 GPa, up to a stress of ≈2.5 GPa, after which small undulations are observed, during both loading and unloading (Fig. 5c). Upon unloading, the undulations *disappear*, again at a stress of ≈2.5 GPa and, as important, *reappear* upon reloading.
iii. linear elastic, followed by pop-ins of the order of ∼2 μm during the first loading cycle (Fig. 5a). While pop-ins do not occur in the second and third cycles, the latter exhibit minor plastic deformation as evidenced by the fact that the loops are slightly open. Subsequent cycles are hysteretic, reproducible and *fully* reversible (inset in Fig. 5a). More importantly the shapes of the repeat stress–strain curves are quite different from those obtained during the first loading. They change from linear elastic with a modulus of 61 GPa, to one that is concave upwards (denoted by short vertical arrow in Fig. 5b, see also inset in Fig. 5b).

It is crucial to note that *only* when loaded to the maximum load of 500 mN, and only in some cases, massive pop-ins were observed. In the absence of such massive pop-ins, and despite the fact that the Hertzian stresses at the tip of the indenter were of the order of 8 GPa or more (Fig. 5b), typically *no trace* of the indentations was found in the SEM. In other words, the indentation marks were only observed in the SEM after massive pop-ins.

4.2. Grade B

Like grade A when grade B samples were indented up to 100 mN, the behavior was completely elastic (Fig. 4a). Indentations to 500 mN resulted in massive, sudden and irreversible

penetrations of the order of 2 μm (Fig. 6a). When the results were converted to NI stress–strain curves, an elastic region, up to about 8 GPa (Fig. 6b), was clearly observed, which was followed by massive pop-ins. Upon reloading, the second cycle showed small amounts of plastic deformation followed by the formation of fully reversible, reproducible loops. Interestingly, W_d for the steady-state indentation loops were slightly greater for grade B than grade A. As observed in grade A, the shape of the stress–strain curves during initial *reloading* in the later cycles is $<<61$ GPa.

To better understand the pop-in events, three different locations on a grade B sample were indented with a sharper, 5 μm, tip up to a load of 200 mN (inset of Fig. 6c). The resulting stress–strain curves were unlike any other, because after the massive pop-ins, somewhat surprisingly, the response remained linear elastic! Very similar results (not shown) were obtained on the A and C micas as well when the 5 μm tip was used.

4.3. Grade C

When grade C samples were loaded to 500 mN, typically one large pop-in followed several smaller pop-ins (denoted by horizontal arrows) during the first cycle (Fig. 7a). When the results were converted to NI stress–strain curves (Fig. 7b), the initial slope on loading corresponded to a modulus of 61 GPa. In contrast to the other grades, however, a yield point was observed between ~1 and 2 GPa, followed by a region of strain-hardening, which was followed by a massive pop-in event (Fig. 7b).

Also unlike the other grades, when loaded to 100 mN, the cyclic load-displacement curves showed hysteresis loops (Fig. 4a). Despite the absence of large pop-ins, here fully reversible loops were observed after the first cycle (Fig. 7b). Note the reproducibility of subsequent cycles and how the elastic regime matches with the first cycle, during reloading. The end of linear elastic behavior

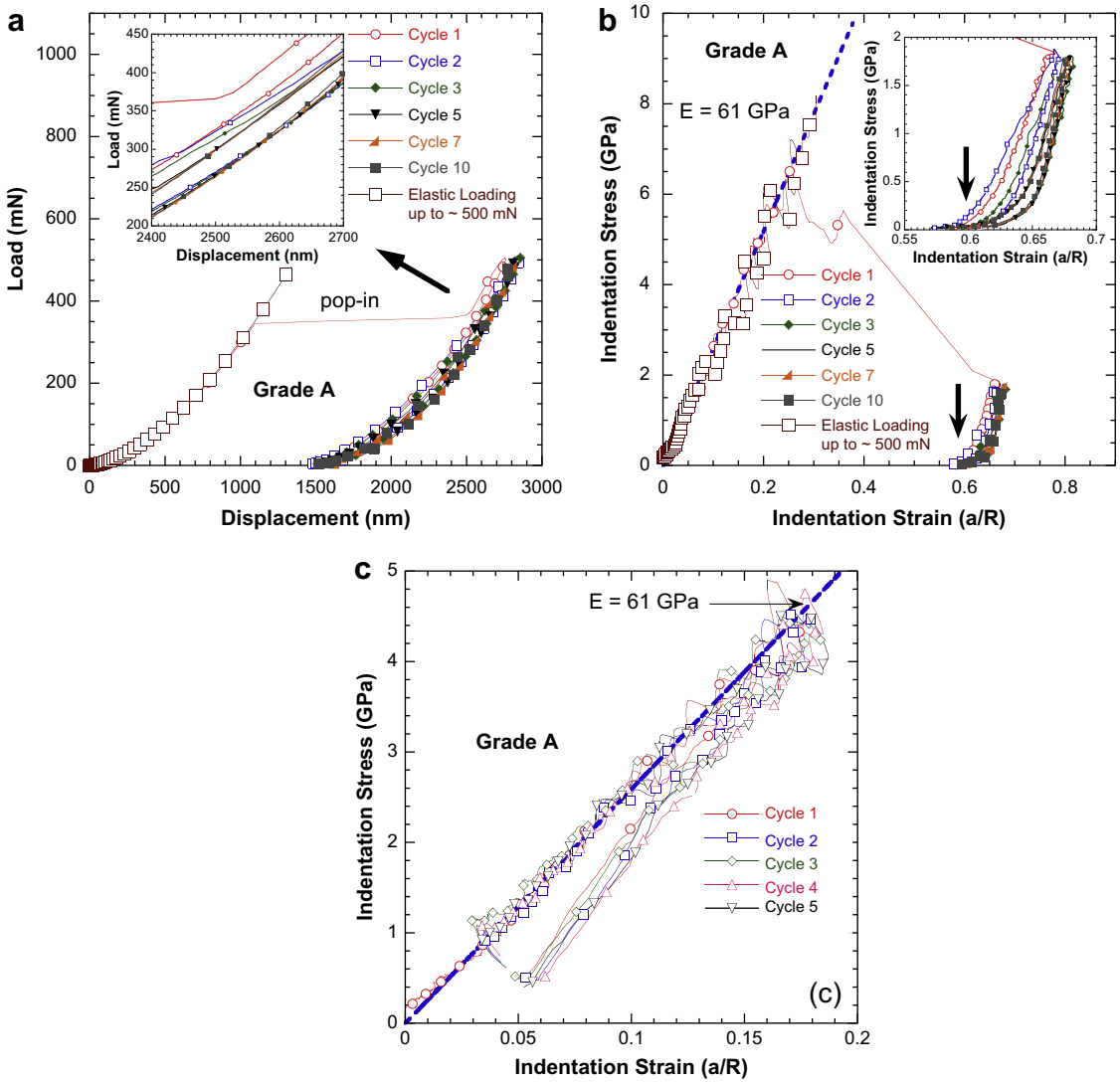

Fig. 5. a) Spherical nanoindentation load-displacement response of grade A mica when a 13.5 μm indenter loaded up to 500 mN. In some locations, large pop-ins were observed, whereas, some locations were elastic up to 500 mN (open squares). The inset magnifies the deformation during cyclic loading. Note that cycles 5–10 are almost identical and show repeatable hysteretic behavior. b) Indentation stress–strain curves for the load-displacement data shown in (a). Note linear elastic behavior prior to the pop-ins with a slope that corresponds to a modulus of 61 GPa (dashed inclined line). The inset illustrates the reversible nature of deformation during cyclic loading after the pop-in. The short vertical arrows highlights the lower modulus obtained during initial loading after pop-ins. c) Indentation stress–strain response when the 13.5 μm indenter was loaded to 100 mN. The linear elastic behavior is represented by the inclined dashed line. Although the deformation is almost elastic for 5 cycles, note reproducible appearance and disappearance of small undulations during loading and unloading, respectively. The residual deformation at the end of each cycle is due to instrumental drift.

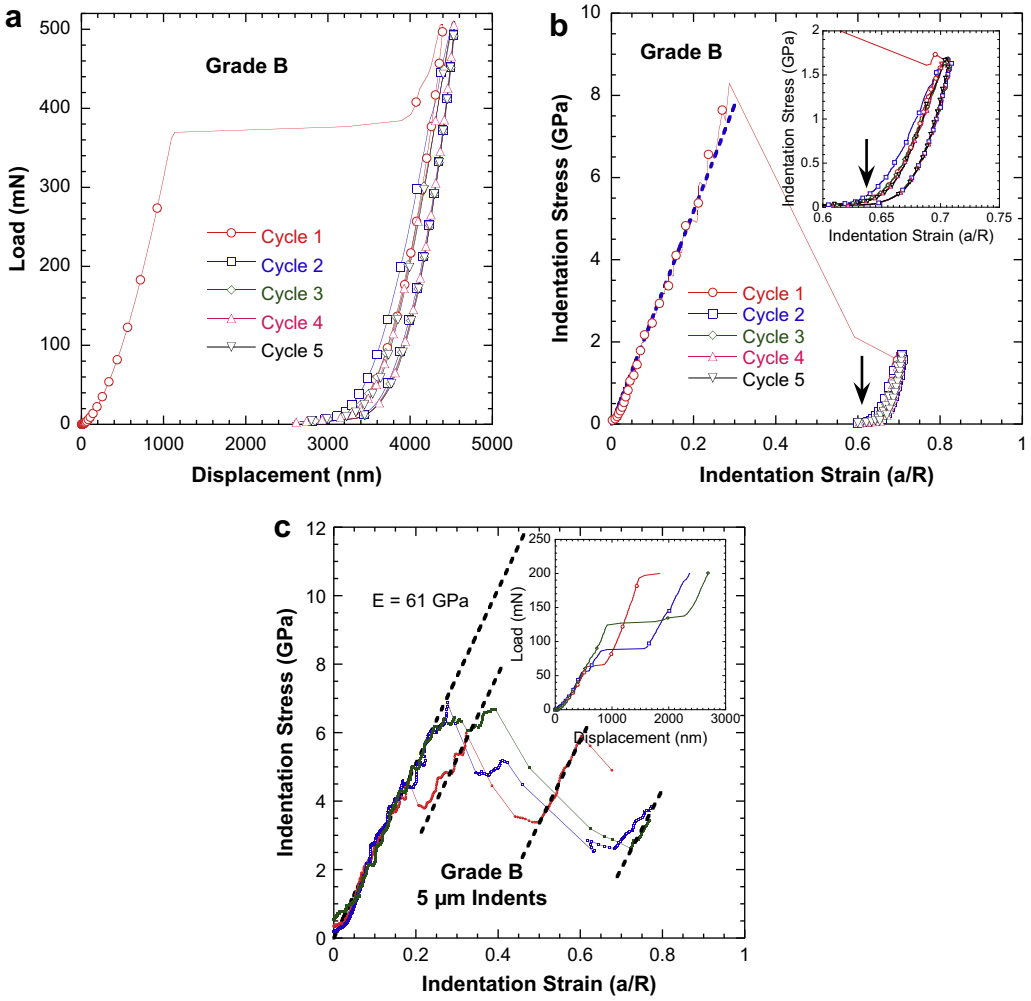

Fig. 6. a) Typical load-displacement response of grade B mica when a 13.5 μm indenter was cycled 5 times to 500 mN in the same location. b) Indentation stress–strain curves for the data in (a). Dashed inclined line represents a modulus of 61 GPa. Inset illustrates the reversible nature of the deformation during cyclic loading after the pop-ins. The short vertical arrows highlights the lower modulus obtained during initial loading after pop-ins. c) The indentation stress–strain response at three different locations, when grade B was indented with a 5 μm indenter to a load of 200 mN. The dashed inclined lines represent linear elastic behavior. Inset shows corresponding load-displacement curves. Note the elastic nature of deformation even after the large pop-ins. Similar behavior was also observed in grades A and C samples.

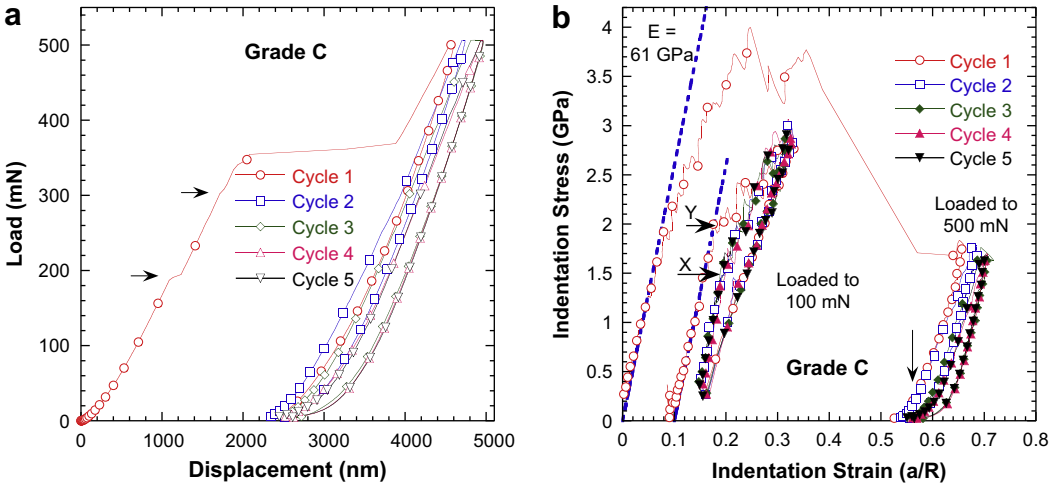

Fig. 7. a) Typical spherical nanoindentation load-displacement response for grade C mica, when a 13.5 μm indenter was loaded up to 500 mN. Note the smaller pop-in events (horizontal arrows) prior to the large pop-in and large hysteretic reversible loops during cyclic loading for 5 cycles. b) Indentation stress–strain curves for the data in (a). Also plotted are the indentation stress–strain curves for loads up to 100 mN. The latter are shifted by 0.1 to the right for clarity of illustration. The dashed inclined lines represent a modulus of 61 GPa. Note, unlike grades A and B, the plastic deformation starts prior to the pop-in (short horizontal arrows). Also important is the fact that in the absence of a pop-in, the initial slope upon reloading is again 61 GPa. The short vertical arrow highlights the much lower slopes of the initial part of the repeat loading after the pop-in.

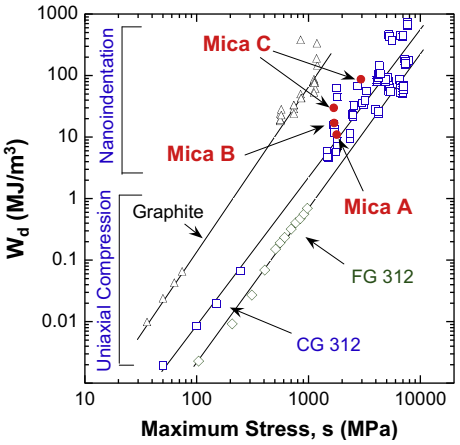

Fig. 8. Log–log dependence of dissipated energy, W_d, on stress for the 3 grades of mica tested here. Also included are the results for graphite and fine-grained (FG) and coarse-grained (CG) Ti_3SiC_2 obtained from both bulk deformation and spherical nanoindentation.

(i.e. deviation from linear elastic curve of 61 GPa) for the repeat cycles is indicated by X in Fig. 7b.

Fig. 8 is a log–log plot of W_d versus applied stress for the various grades of mica tested here. Also in Fig. 8 are the results for Ti_3SiC_2 and graphite for comparison with other KNE solids (Barsoum et al., 2005b). This plot illustrates that KNE behavior is not only limited to sheet silicates, but is observed in other materials as well.

5. Discussion

5.1. Indentation stress–strain behavior

The most important finding of the present investigation, and the one that has the most bearing on geology, is the crucial role of defects in the deformation behavior. The highest quality mica, grade A, is clearly the most immune to kinking; in some cases, even at stresses up to ~8 GPa, the response was linear elastic (e.g. open squares in Figs. 5a, b). Similarly, the response of the grade B samples resulted in either fully reversible hysteretic loops, after small pop-ins in the first cycle (Barsoum et al., 2004b), or large pop-ins of the order of 2 μm at stresses, again, of the order of 8 GPa (Fig. 6b).

Recent *ab initio* and molecular dynamics calculations (Roundy et al., 1999) have shown that dislocations in *perfect* metal crystals nucleate when:

$$\tau_{max} \approx \sigma/2 = G/n \qquad (13)$$

where n is a real number of the order of 10. τ_{max} and σ are the shear and normal contact stresses under the indenter, respectively. Assuming that the appropriate shear modulus in this case is not G, but c_{44}, which for muscovite mica is 15 GPa (McNeil and Grimsditch, 1993), and considering that the pop-in stresses occur at a $\sigma \approx 8$ GPa for grade A, it follows that in this case n is ~4. In general, it is not easy to experimentally determine n. The fact that this value is close to the theoretical strength and can be readily measured here is one of several advantages of using spherical NI and converting the results to stress–strain curves (Basu and Barsoum, 2007; Basu et al., 2006a). This comment notwithstanding, more work is ongoing and needed to understand the dislocation nucleation process during the massive pop-in events commonly observed when spherical, rather than sharp, nanoindenters are used.

In contrast to grades A and B, the "yield point" of grade C (point Y in Fig. 7b) is roughly four times smaller than the pop-in stresses for micas A and B (Figs. 5b and 6b). This result is consistent with the fact that grade C, with its high initial defect concentration, either does not need to nucleate dislocations during the first cycle because they are presumably already present, and/or the defects significantly lower the barrier to their nucleation.

Grade C, with the most defects, was not only the mica type where kinking occurred most readily at the lowest stresses (Fig. 7b), but also where the most stochastic response was observed (Fig. 4c), most probably reflecting the distribution of flaws in that material. For example, two different regions clearly registered quite different average pop-in stresses. At this time, the nature of the defects responsible for catalyzing IKB formation has not been identified. Further in-situ TEM studies are needed to shed light on the mechanisms operating here.

The 100 mN indentation results for grade C mica (Fig. 7b), wherein no large pop-ins were observed, are most readily explained by our KB-based model. During the first cycle, at a yield point (indicated by Y in Fig. 7b) of ~2 GPa, dislocations, most probably in the form of mobile dislocation walls, MDWs (Fig. 1b), start moving away from each other and subsequently form permanent KBs, which in turn leads to strain-hardening. The latter explains the increase in stress with strain, observed beyond the yield point in Fig. 7b. On reloading, IKBs form, but presumably only in between the kink boundaries formed during the first cycle. Note that the yield point during the repeat cycles (indicated by X in Fig. 7b) is lower than the first cycle. The fact that the slope of the initial part of the stress–strain curves during *repeat* cycles agrees with the elastic modulus (~61 GPa) is noteworthy and is important evidence that delaminations do *not* play a role in this case.

Note dislocation glide on different slip systems cannot explain this phenomenon. Were the dislocations allowed to entangle, the process would not be reversible (Bell and Wilson, 1981; Kronenberg et al., 1990; Meike, 1989). We do not rule out the possibility that interactions between dislocations on the *same* basal plane do not occur. They probably do, but if they occur, they would have to be reversible as well.

The results for the 500 mN indents (Figs. 5b, 6b and 7b) can also be explained by our model, by postulating that the pop-ins are caused by delaminations as a result of tensile stresses (Eq. (7)). Here, during the pop-in, deformation changes from initially elastic to one that is hysteretic so that the second and third cycles are slightly open, but all subsequent cycles to the same stress level are fully reversible (Figs. 5b, 6b and 7b). As discussed above, this sequence of events has been linked to the presence of three interrelated microscopic events (Fig. 1a–c):

a) during the pop-ins, the stored elastic energy is converted to multitudes of dislocations in the form of MDWs, that, in turn, form KBs;
b) KBs lead to the formation of a multiplicity of smaller domains under the indenter; and
c) IKBs form within the smaller domains during the repeat cycles resulting in fully reversible hysteretic loops. Direct evidence for the breakdown into small domains of what was initially a single crystal is obvious from the SEM micrographs (Fig. 3).

The important role of delaminations for the 500 mN loading case is best evidenced by the shape of the stress–strain curves upon reloading. They are concave upward during the *initial* parts of the repeat loadings (vertical arrows, Figs. 5b, 6b and 7b). It is reasonable to assume that during the initial re-loadings the indenter tip closes the delaminations/cracks, resulting in lower stiffness.

Contrast this response to the 100 mN loading case (Fig. 7b), where delaminations are inferred to be absent. Consistent with this interpretation is the fact that a *higher* stress is actually sustained

when the indenter is loaded to 100 mN, as compared to a load of 500 mN during the repeat cycles. This somewhat paradoxical situation is a direct result of the massive pop-ins sustained at 500 mN, and the formation of relatively large craters (Fig. 3c).

Other evidence that delaminations play a role can be seen in Fig. 5c, where the small undulations, introduced during loading, disappear upon unloading. These tiny undulations, or pop-ins, are believed to be associated with delaminations underneath the indenter and are believed to heal upon removal of the load, because they are not exposed to the atmosphere (Lawn and Wilshaw, 1975). The excellent reproducibility of the stress–strain curves (Fig. 5c), where many fine features recur, repeatedly at roughly the same stresses, from cycle to cycle is consistent with such an interpretation. Note that at lower stresses, the undulations disappear, only to reappear at higher stresses.

Fig. 6c also clearly demonstrates the formation of delaminations during the pop-in events. When indented with the 5 μm indenter tip, multiple pop-in events occur successively, interspersed by regions in which the response appears to be purely *elastic*. Consistent with this interpretation is the fact that these multiple pop-in events are much more common with the "sharper" – i.e. 5 μm radius – of the two indenters (Fig. 6c). Note that during indentation, folding of the basal planes occurs due to localized bending. At first, the bending stress on the basal planes is elastic, but at greater stresses the basal planes rupture in a stochastic process, giving rise to multiple pop-in events in the NI experiments.

As noted above, delaminations are inherent to the IKB to KB transformation because without them, it would be impossible for the material to pile-up around the indentation mark as observed (Fig. 3). Note that basal-plane dislocation arrays (Christoffersen and Kronenberg, 1993) are also inherent to the overall process because without them, the basal planes could not shear relative to each other.

5.2. Estimation of CRSS from energy dissipation per cycle, W_d

To better understanding the kinking of mica, it is instructive to study the microscale deformation in light of our theoretical model, described in Section 2.1. To verify our model, we should first estimate the threshold stresses for IKB nucleation. The threshold stress is the value at which the response on reloading is no longer linear elastic. For example, in the 100 mN case in Fig. 7b, that stress is denoted by a short arrow labeled X and is estimated to be $\sim 1.6 \pm 0.1$ GPa. Using this value in Eq. (1), the domain size 2α is estimated to be $\sim 13 \pm 2$ nm. And although the number is small, it is reasonable considering the size of the indent and the stresses applied.

To estimate the CRSS, or Ω/b, for basal plane dislocations comprising the IKBs, we also need to have a closer look at W_d during the repeat cycles. Because of the high stresses possible under the nanoindenter, W_d is of the order of $\approx$10–90 MJ/m^3 (Fig. 8). It is also evident that grade C dissipates the most energy as compared to the other grades, specially in the *absence* of pop-ins (see 100 mN loading case in Fig. 7b), where W_d is estimated to be $\approx$90 MJ/m^3. As a check on these values, we note that when the area enclosed by the load-displacement curve (Fig. 7a) is divided by a^3 – assuming that is roughly the volume affected by NI – a value of $\approx$85 MJ/m^3 is obtained. In other words, the two values are quite close. This is important because it indirectly validates our methodology for generating the NI stress–strain curves and also confirms that the area affected by the NI is of the order of a^3.

There are several methods by which one can estimate Ω/b. In this work, we use the relationship between W_d and σ (Eq. (6). Assuming $N_k\alpha^3 = 1$, and $\sigma_t = 1.6 \pm 0.2$ GPa, the CRSS, or more exactly Ω/b, is estimated to be $\approx 81 \pm 5$ MPa. In a recent paper on cyclic NI of $LiNbO_3$ (Basu et al., 2008), we have shown that $N_k\alpha^3$ can vary between 1 and 6. If $N_k\alpha^3 = 3$ is assumed, then $\Omega/b = 27 \pm 2$ MPa, a value that is comparable to the 20–30 MPa CRSS values obtained for biotite in triaxial experiments (Kronenberg et al., 1990). These results notwithstanding, more work is required to better relate the energy dissipated under a spherical NI with bulk CRSS values.

5.3. Geological implications

Deformation by kinking in geological solids, especially layered silicates, is well known. In this, and previous work (Barsoum et al., 2004b, 2003, 2005b), we made the point that IKBs are the precursors of KBs, such that KBs cannot form without IKBs. This work clearly shows that the quality of the mica dictates the threshold stresses at which the IKBs, and in turn, the KBs form.

Some may argue that while this work is interesting it is of little use to structural geologists since the deviatoric stresses estimated here – of the order of 80 MPa – are greater than those often encountered in geologic formations. And while at face value this reasoning makes sense, nevertheless this work is still quite relevant for several reasons with one caveat: the usefulness of the value of the CRSS calculated herein. It is important to note in this context that, although NI experiments somewhat mimic the triaxial stress states in geological formations, more work is needed to correlate CRSS calculated from NI to the values obtained from bulk experiments.

The first reason for the geological relevance of these results is the most direct: kink bands exist in nature and thus must IKBs. To understand the former, one needs to understand the latter.

The second reason is that, in a geologic formation, as in a polycrystalline material, the concentration of IKB nucleating defects is presumably large enough as to nucleate the IKBs at much lower stresses than the ones reported here. For example, we have shown that the threshold stresses needed for IKB nucleation in polycrystalline graphite is roughly an order of magnitude lower than in single crystal graphite. The same is true for a mica-containing glass ceramic (Zhen, 2004) and for Mg (Basu and Barsoum, unpublished results). Even more relevant, this work shows that simply changing the mica quality can reduce the threshold stresses from over 8 GPa in some cases to $\sim$1.6 GPa. Delaminations, microcracks and basal plane ruptures must also play an important role in reducing threshold stresses.

The third reason is that the formation of KBs by no means implies that IKBs cease to exist or nucleate. If that were the case, then no reversible loops in the indentation stress–strain plots (Figs. 5b, 6b and 7b) would have been observed *after* the pop-ins. Our results are consistent with the idea postulated by Hess and Barrett (1949) that IKBs will nucleate within KBs after the formation of the latter (Fig. 1c). For example, the larger 100 mN reversible loops (Fig. 7b) are ones that we believe form due to IKBs within the 13 nm domains created during the first cycle. If one excludes non-basal slip, then the domain walls have to be kink boundaries.

Lastly, in addition to their importance in nucleating kink bands, IKBs have important characteristics in their own right. Depending on their density, they significantly increase the "elastic" energy stored in a given formation. This extra stored energy ($=\frac{1}{2}\,\varepsilon_{NL}\sigma$) is *not* in the form of stretched atomic bonds, however, but rather in stacked dislocation loops. When the pressure is relieved some of that energy is imparted back to the surroundings and some, viz. $W_d/2$, is dissipated as heat.

We have also shown that nonlinear dynamic effects occur due to the interaction of dislocations with sound waves (Barsoum et al., 2005a). It follows that a lithology rich in KNE minerals that had been deformed and/or is under deviatoric stress will interact

differently with sound waves than a KNE-poor lithology or a KNE-rich lithology that had not been deformed. This study, as our previous one (Barsoum et al., 2004b), can be related to the phenomenological models, assuming discreet elastic elements, proposed for hysteretic deformation in geological materials (Guyer and Johnson, 1999; Guyer et al., 1995).

6. Conclusions

We studied the deformation behavior in muscovite mica, with different initial defect concentrations, by cyclic spherical NI. Using our indentation stress–strain analysis and dislocation-based microscale model we reach the following conclusions:

a) The nucleation of KBs, formed during the deformation of layered silicates, can be explained by dislocation-based IKBs.
b) The threshold stress for the formation of IKBs depends on initial defect population and domain size.
c) After formation, the IKBs can grow and shrink reversibly and hence dissipate a large amount of energy because of the to-and-fro motion of the dislocations loops that comprise them.
d) At greater stresses, IKBs devolve, first into MDWs, which with increasing stress transform into kink boundaries. Basal plane delaminations and/or rupturing are concomitant with this transformation process. And,
e) Spherical NI approximately mimics the geological conditions deep inside the earth and hence the NI stress–strain analysis can provide important information regarding the elasto-plastic deformation of minerals under such conditions.

References

Barsoum, M.W., El-Raghy, T., 1999. Room temperature ductile carbides. Metall. Mater. Trans. 30A, 363–369.
Barsoum, M.W., Farber, L., El-Raghy, T., Levin, I., 1999. Dislocations, kink bands and room temperature plasticity of Ti_3SiC_2. Metall. Mater. Trans. 30A, 1727–1738.
Barsoum, M.W., Murugaiah, A., Kalidindi, S.R., Gogotsi, Y., 2004a. Kink bands, nonlinear elasticity and nanoindentations in graphite. Carbon 42, 1435–1445.
Barsoum, M.W., Murugaiah, A., Kalidindi, S.R., Zhen, T., 2004b. Kinking nonlinear elastic solids, nanoindentations and geology. Phys. Rev. Lett. 92, 255508–255511.
Barsoum, M.W., Radovic, M., Zhen, T., Finkel, P., 2005a. Dynamic elastic hysteretic solids and dislocations. Phys. Rev. Lett. 94, 085501.
Barsoum, M.W., Zhen, T., Kalidindi, S.R., Radovic, M., Murugahiah, A., 2003. Fully reversible, dislocation-based compressive deformation of Ti_3SiC_2 to 1 GPa. Nat. Mater. 2, 107–111.
Barsoum, M.W., Zhen, T., Zhou, A., Basu, S., Kalidindi, S.R., 2005b. Microscale modeling of kinking nonlinear elastic solids. Phys. Rev. B. 71, 134101.
Basu, S., Barsoum, M.W., 2007. Deformation micromechanisms of ZnO single crystals as determined from spherical nanoindentation stress–strain curves. J. Mater. Res. 22 (9), 2470–2477.
Basu, S., Barsoum, M.W., Kalidindi, S.R., 2006a. Sapphire: a kinking nonlinear elastic solid. J. Appl. Phys. 99, 063501.
Basu, S., Moseson, A., Barsoum, M.W., 2006b. On the determination of spherical nanoindentation stress strain curves. J. Mater. Res. 21 (10), 2628–2637.
Basu, S., Zhou, A., Barsoum, M.W., 2008. Reversible dislocation motion under contact loading in $LiNbO_3$ single crystal. J. Mater. Res. 23, 1334–1338.
Bauer, M., 1874. Uber einige physikalische verhaltnisse des glimmers. Z. Dtsch. Geol. Ges. 26, 137–180.
Bell, I.A., Wilson, C.J., 1981. Deformation of biotite and muscovite: TEM microstructure and deformation model. Tectonophysics 78, 201–228.
Christoffersen, R., Kronenberg, A.K., 1993. Dislocation interactions in experimentally deformed biotite. J. Struct. Geol. 15, 1077.
Farber, L., Levin, I., Barsoum, M.W., 1999. HRTEM study of a low-angle boundary in plastically deformed Ti3SiC2. Phil. Mag. Lett. 79, 163.
Field, J.S., Swain, M.V., 1995. Determining the mechanical-properties of small volumes of material from submicrometer spherical indentations. J. Mater. Res. 10 (1), 101–112.
Frank, F.C., Stroh, A.N., 1952. On the theory of kinking. Proc. Phys. Soc. 65, 811–821.
Guyer, R.A., Johnson, P.A., 1999. Nonlinear mesoscopic elasticity: evidence for a new class of materials. Phys. Today 52 (4), 30–36.
Guyer, R.A., McCall, K.R., Boitnott, G.N., 1995. Hysteresis, discrete memory and nonlinear wave propagation in rock: a new paradigm. Phys. Rev. Lett. 74, 3491.
Herbert, E.G., Pharr, G.M., Oliver, W.C., Lucas, B.N., Hay, J.L., 2000. On the measurement of stress–strain curves by spherical indentation. In: Baker, S.P., Cook, R.F., Corcoran, S.G., Moody, N.R. (Eds.), Fundamentals of Nanoindentation and Nanotribology II. MRS, Boston, MA, p. 649. Q3.4.1.
Hertz, H., 1896. Miscellaneous Papers by H. Hertz. Macmillan, London.
Hess, J.B., Barrett, C.S., 1949. Structure and nature of kink bands in zinc. Trans. AIME 185, 599–606.
Holcomb, D.J., 1981. J. Geophys. Res. 86, 6235.
Johnson, K.L., 1985. Contact Mechanics. Cambridge University Press, Cambridge.
Kronenberg, A., Kirby, S., Pinkston, J., 1990. Basal slip and mechanical anisotropy in biotite. J. Geophys. Res. 95, 19257.
Lawn, B.R., Wilshaw, T.R., 1975. Fracture of Brittle Solids. Cambridge University Press, Cambridge, UK.
Mares, V.A., Kronenberg, A.K., 1993. Experimental deformation of muscovite. J. Struct. Geol. 15, 1061–1075.
McCall, K.R., Guyer, R.A., 1994. Equation of state and wave propagation in hysteretic nonlinear elastic materials. J. Geophys. Res. 99 (B12), 23887–23897.
McNeil, L.E., Grimsditch, M., 1993. Elastic moduli of muscovite mica. J. Phys. Condens. Matter 5, 1681–1690.
Meike, A., 1989. In situ deformation of micas: a high-voltage electron-microscope study. Am. Mineral. 74, 780.
Moseson, A., Basu, S., Barsoum, M.W., 2008. Determination of the effective zero point of contact for spherical nanoindentation. J. Mater. Res. 23 (1), 204–209.
Roundy, D., Krenn, C.R., Cohen, M.L., Morris Jr., J.W., 1999. Ideal shear strengths of fcc aluminum and copper. Phys. Rev. Lett. 82 (13), 2713–2716.
Shea, W.T., Kronenberg, A.K., 1993. Strength and anisotropy of foliated rocks with varied mica contents. J. Struct. Geol. 15, 1097–1121.
Stroh, A.N., 1958. The cleavage of metal single crystals. Philos. Mag. 3, 597.
Tabor, D., 1951. Hardness of Metals. Clarendon, Oxford, U.K.
Weibull, W., 1951. A statistical distribution function of wide applicability. J. Appl. Mech. 18, 293–297.
Zhen, T., 2004. Compressive Behavior of Kinking Non-linear Elastic Solids – Ti3SiC2, Graphite, Mica and BN. PhD thesis, Drexel University.
Zhen, T., Barsoum, M.W., Kalidindi, S.R., 2005. Effects of temperature, strain rate and grain size on the mechanical compressive properties of Ti_3SiC_2. Acta Mater. 53, 4163–4171.
Zhou, A., Basu, S., Barsoum, M.W., 2008. Kinking nonlinear elasticity, damping, micro- and macroyielding of hexagonal close-packed metals. Acta Mater. 56 (1), 60–67.
Zhou, A.G., Barsoum, M.W., Basu, S., Kalidindi, S.R., El-Raghy, T., 2006. Incipient and regular kink bands in dense and 10 vol.% porous Ti2AlC. Acta Mater. 54, 1631.